Heliyon 10 (2024) e27010

Contents lists available at ScienceDirect

Heliyon

journal homepage: www.cell.com/heliyon

Research article

Interfacial reaction of Sn-1.5Ag-2.0Zn low-silver lead-free solder with oriented copper

Jin Xiao[a,b,*], Wei Cheng[c], Qu Fu-kang[a]

[a] School of Mechanical and Electrical Engineering, Guangzhou Huali College, Guangzhou, 511300, China
[b] School of Advanced Manufacturing, Guangdong Songshan Polytechnic College, Shaoguan, 512126, China
[c] School of Intelligent Equipment Manufacturing, Zhongshan Torch Polytechnic College, Zhongshan, 528436, China

ARTICLE INFO

Keywords:
Sn-1.5Ag-2.0Zn
Single crystal
Copper alloy solder
Soldering
Diffusion

ABSTRACT

High density packaging technology reduces the pad size and the number of grains contained in the pad. When the polycrystalline pad turns into a single crystal pad, the grain orientation has an important impact on the formation of the intermetallic compound (IMC) at the interface. The growth of IMC at the interface between the solder and the single-crystal copper substrate is investigated by selecting the prospective Sn-1.5Ag–2Zn as the solder alloy. Sn-1.5Ag-2.0Zn lead-free solder joints soldered with single crystal (111) copper substrate and polycrystalline red copper substrate are reflowed at 250 °C for 5 min. Samples are subsequently aged at 160 °C. The uneven scallop like Cu_6Sn_5 IMC layer grows rapidly when the alloy solder contacts with the copper substrate. The Cu_6Sn_5 grain size formed on the surface of single crystal copper is larger than that of polycrystalline copper. Single crystal copper has no grain boundary to block atomic diffusion, which affects grain nucleation and growth. The growth rate of Cu_6Sn_5 formed by alloy solder and the single crystal (111) copper solder joint after aging treatment at 160 °C for 20 h is about twice that of the polycrystalline copper solder joint. Then it grows slowly with the increase of aging treatment time. The thick layer Cu_6Sn_5 breaks due to crack diffusion after 600 h of aging treatment, and the thickness of IMC remains at 3.5 μm. Cu_5Zn_8 generated at the solder and polycrystalline copper solder joint during aging treatment acts as a barrier layer, preventing the solder from contacting the copper substrate and inhibiting the formation of Cu_6Sn_5. Cu_5Zn_8 is broken and decomposed after 300 h of aging treatment, and Cu_6Sn_5 grows rapidly after the barrier layer disappeared. The thickness of Cu_6Sn_5 is about 2.8 μm. The thickness of IMC of solder joint on single crystal copper is 0.7 μm more than that on polycrystalline copper. After aging treatment, the IMC formed at the interface between alloy solder and single crystal copper has better compactness and basically no pores, while there are obvious pores between IMC grains at the interface between alloy solder and polycrystalline copper, which can predict that the soldering quality of the interface between alloy solder and single crystal copper is better. This will provide application prospects for solder joint interface reliability research.

1. Introduction

Eutectic tin-lead solder has low melting point, low cost and excellent performance. It has been commonly used in the field of

* Corresponding author. 11 Huali Rd., Zengcheng District, Guangzhou Huali College, Guangzhou 511300, China.
E-mail address: 67104869@qq.com (J. Xiao).

https://doi.org/10.1016/j.heliyon.2024.e27010
Received 19 July 2023; Received in revised form 21 February 2024; Accepted 22 February 2024
Available online 28 February 2024

electronic packaging. However, the lead decomposed from tin-lead solder in electronic products pollutes the environment and threatens human health [1–6]. Moreover, the poor thermal workability and creep resistance of tin-lead solder cannot meet the requirements of packaging technology development. Researchers have been searching for lead-free solders that can match the performance of Sn–Pb solders [7–10]. The Sn–Ag system is currently recognized as the most desirable lead-free solder. It is stronger and more creep resistant than Sn–Pb solder. However, the solder has a high melting point and is costly [11–14]. Many studies have been conducted to improve the wettability and reduce the melting point by adding Cu, Zn, Ni, Bi and other components to Sn–Ag solder [15–20]. Sn-3.5Ag is the most commonly used lead-free solder with high Ag content and high cost. The cost of silver accounts for more than half of the cost of the solder. The intermetallic compounds (IMCs) Ag_3Sn and Cu_6Sn_5 at the solder joints are in coarse slats after aging of the solder. They are brittle and affect reliability [21–26]. Low silver content solder can reduce the cost of solder. It also brings the problems of melting properties and strength reduction [27,28]. Hammad et al. found that granular Ag_3Sn at the solder joint improved the mechanical strength of the solder and lamellar Ag_3Sn had poor plastic deformation [29,30]. Sn–Ag solder with trace additive Zn formed Sn–Ag–Zn solder with low tin cost, environmental friendliness and good wettability. It had been reported that filling with Zn can change the dendrite organization and form finer eutectic in the matrix [31,32]. Ramos et al. found that the addition of 0.1–0.7% Zn as an alloying element in SAC305 solder can reduce subcooling [33,34]. The formation of IMC in large Ag_3Sn plates was inhibited. Wei et al. showed that the addition of 0.1–0.3% Zn particles resulted in a slight decrease in the thickness of IMCs [35]. The addition of 0.3% Zn did not affect the tensile and impact strength, however further addition deteriorated them. Creep resistance kept increasing as the tin solder increases to 0.9% [36].

As the packing density increases, the solder contact copper layer will shrink from polycrystalline to monocrystalline. Intermetallic grains become a key issue in three-dimensional packaging. The morphology of Cu_6Sn_5 IMC grains depends on the orientation of the Cu layer. The grain orientation of copper has an important influence on the morphology of interfacial IMCs as well as on the disposition, and interfacial Cu_6Sn_5 grains with highly anisotropic morphology and orientation will significantly affect the reliability of micro solder joints [37]. Qiao et al. studied the solid-liquid interface between lead-tin solder and single crystal copper [38]. It was found that the grain growth mode of Cu_6Sn_5 was related to the oriented copper crystal plane. Ma et al. studied the morphology and phase of Cu_6Sn_5 formed by Sn–Ag–Cu solder and (001) oriented copper [39]. The orientation and size of Cu_6Sn_5 can be controlled at different stages of reflow soldering. Dong etc. used multiple reflow processes and found that the interface between Sn–3Ag solder and (001) Cu single crystals formed the orientation-preferred Cu_6Sn_5 by grain rotation and engulfment, and the Cu_6Sn_5 morphology shifted from a fan shape to a small surface, which was beneficial for improving the reliability of the solder joints [40].

Current research on Sn–Ag–Zn solder systems has focused on the vicinity of the eutectic composition, while few low-Ag content Sn–Ag–Zn solders have been reported. This paper synthesizes the cost advantages, meltability, and wetting properties of low-silver solder and the promising Sn-1.5Ag-2.0Zn solder was selected. The Sn-1.5Ag-2.0Zn alloy solder was soldered to an oriented single crystal copper substrate. The IMC species and properties at the interface between the solder joints and different substrates were observed and studied under reflowing at 250 °C with different aging treatment conditions. The grain size of Cu_6Sn_5 on different copper substrates varied significantly. The grain size of Cu_6Sn_5 generated at the Sn-1.5Ag-2.0Zn/single crystal copper substrate solder joints was about 2.6 μm, about twice that of polycrystalline copper. The Cu_5Zn_8 IMC barrier layer generated at the Sn-1.5Ag-2.0Zn/polycrystalline copper substrate solder joints during heat treatment at 160 °C inhibited the generation of Cu_6Sn_5. The Cu_6Sn_5 IMC at the Sn-1.5Ag-2.0Zn/single-crystal copper substrate solder joint grew slowly with time under 160 °C heat treatment, with a thickness of about 3.5 μm, while the commercially available solder SAC305 generated IMCs up to 7.28 μm. The thickness of the IMC generated by Sn-1.5Ag-2.0Zn with the copper substrate was appropriate, which contributes to the strength and toughness of the solder joint. The IMC was found to collapse after a long heat treatment.

2. Experimental materials and methods

In this paper, a commercial (111) oriented copper round bar (ø20 mm) was selected. The copper sheet was cut into 1 mm thickness copper sheet by wire cutting, and ground with 800#, 1200#, 1600# and 2000# sandpaper in sequence. The copper sheet was polished with the diamond grinding paste, degreased with acetone, cleaned with ultra-pure water and then blown dry.

High-purity (99.99%) tin, silver and zinc pellets were molten directly to obtain Sn–Ag–Zn solder. The raw materials were added to the corundum crucible in a certain mass ratio and molten. The molten temperature was set at 650 °C, the holding time was 40 min, and the alloy liquid was stirred once every 4 min to make a uniform composition. During the holding time, the top of the alloy liquid was covered with LiCl–KCl salt to prevent evaporation and oxidation of the liquid. After cooling, a certain composition of alloy solder was obtained. Alloy solder of 0.5 g was weighed with an electronic balance. It was placed in rosin liquid at 260 °C to prevent its oxidation. The solder molten and formed a sphere due to surface energy, and the alloy solder balls were obtained by cooling in quenching oil. The solder balls were degreased and cleaned for use.

The prepared 0.5 g solder balls were dipped in a small amount of rosin flux and placed on the copper sheet. There are two types of copper sheets. One is the oriented single crystal copper sheet (ø20 mm*1 mm) prepared above. The other is a commercial polycrystalline copper sheet (size 20 mm*20 mm*1 mm). The copper sheets were placed on a constant temperature thermostatic heating plate and heated to 250 °C. The soldering time was set to 5 min. After the specimens were cooled to room temperature, they were cleaned with acetone to remove oil. Referring to the environmental test for electrical and electronic products (Chinese national standard GB/T2423.2), the post-soldering specimens were heated in a constant temperature drying oven with the temperature 160 °C, and the aging time was 20 h, 100 h, 300 h and 600 h, respectively. Fig. 1 shows the schematic diagram of alloy solder and copper substrate.

The reflowed and aged solder joints were sliced vertically and then cold mosaic processed to make cross-sectional specimens. The specimens were polished with 800#, 1200#, 1600#, 2000# sandpaper in sequence, polished with diamond abrasive paste, and then rinsed and blown dry with anhydrous ethanol for preservation after polishing.

The top-view specimens were prepared with sandpaper to pre-sand excess solder to a thin layer. The specimens were then etched in a metallographic etching solution (10% nitric acid solution) until the IMCs at the interface were completely exposed, cleaned and blown dry. The interfacial morphology was observed by a field emission scanning electron microscope (Regulus 8100) with back-scattered electron (BSE) and secondary electron (SE) imaging, an energy spectrometer (Merck EscaLab 250Xi), and an X-ray poly-crystalline diffractometer (Bruker D8 advance) to quantify the tissue composition and elemental distribution at the interface.

In order to better study the changes in the interfacial microstructure of Sn-1.5Ag-2.0Zn solder after soldering and aging treatment, the dimensional thickness of interfacial IMCs and other microstructures were quantitatively characterized during the analysis of interfacial reliability. The characterization method is based on the original SEM photographs. The thickness of interfacial IMCs was measured using the precise measurement function of Adobe Photoshop CS4. The experimental data was the average of the measured values. Three random location morphology photos were selected under the same conditions. Five values were measured randomly in each photo, for a total of 15 measured values. After removing one maximum value and one minimum value the average value was taken as the final measured value experimental data.

3. Results and analysis

3.1. Interface morphology of solder and different copper substrates

Fig. 2(a) shows the interfacial morphology of polycrystalline red copper and Sn-1.5Ag–2Zn solder reflowed at 250 °C for 5 min. Fig. 2(b) shows the interfacial morphology of oriented single crystal copper (111) and Sn-1.5Ag–2Zn solder reflowed at 250 °C for 5 min. It can be seen from the one liner that only one IMC is formed at the interface during reflow soldering.

The IMC layer on the polycrystalline copper was found to be flatter with a thickness of about 1.4 μm. The IMC layer on the oriented single-crystal copper (111) had scallop-type raised structure with a thickness of about 2 μm. The difference in IMC thickness indicates a faster IMC growth rate on single crystal copper under the same reflow conditions. Single-crystal copper had no grain boundaries to hinder atomic diffusion and the IMC grows at a faster rate.

The EDX analysis of points 1 and 2 in Fig. 2 (Table 1) shows that the IMCs at the interface between the solder and the copper substrate were both Cu_6Sn_5. The liner at the interface in Fig. 2 also indicated that only one IMC was formed.

Fig. 3(a) and (b) show the top-view morphology of the polycrystalline, (111)-oriented single-crystal copper substrate with Sn-1.5Ag-2.0Zn at 250 °C with a reflow time of 5 min. It was found that the grain diameter of the Cu_6Sn_5 IMC generated at the interface between the solder and polycrystalline copper was about 1.5 μm, while the grain diameter of the Cu_6Sn_5 IMC generated at the interface between the solder and (111) single-crystal copper was significantly larger than that of the IMC at the polycrystalline copper interface, which was about 2.6 μm. This is due to the fact that single-crystal copper does not have grain boundaries while polycrystalline copper has grain boundaries. The presence of an interface at the grain boundary can facilitate nucleation. The nucleation rate at the interface of single-crystal copper was much lower than that of polycrystalline copper. The growth process of Cu_6Sn_5 IMC was accompanied by atomic diffusion. The grain boundaries in polycrystalline copper acted as a barrier to atomic diffusion, while single-crystal copper had no grain boundaries to impede atomic diffusion. This resulted in significant variability in grain size of Cu_6Sn_5 IMC on different copper substrates. Fig. 3(c) shows the XRD analysis diffraction pattern of the top view interface formed by the alloy solder and (111) single crystal copper. It was found that the IMCs at the interface were Cu_6Sn_5 and Ag_3Sn, and there were small white nanoscale particles between the Cu_6Sn_5 grains on the surface of Fig. 3(b), which, combined with the XRD analysis, should be Ag_3Sn small particles.

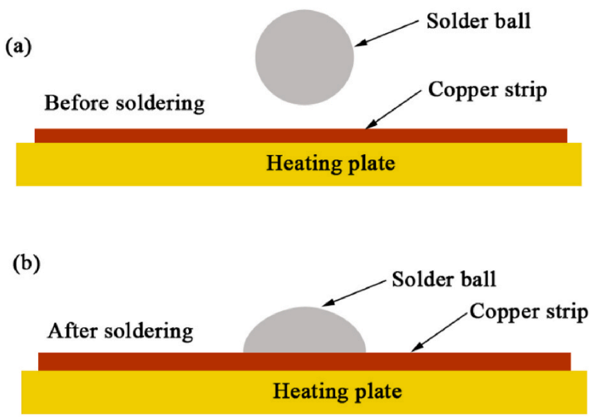

Fig. 1. Schematic diagram of alloy solder and copper substrate soldering: (a) before soldering (b) after soldering.

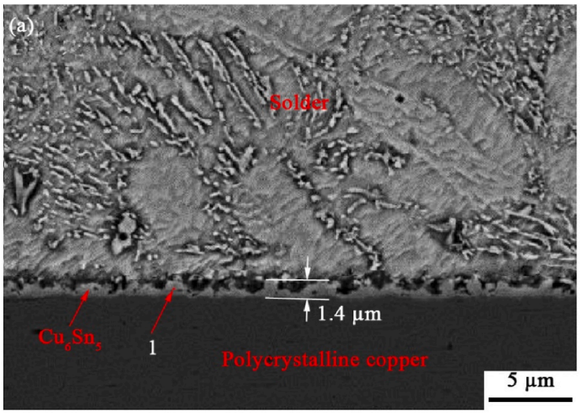

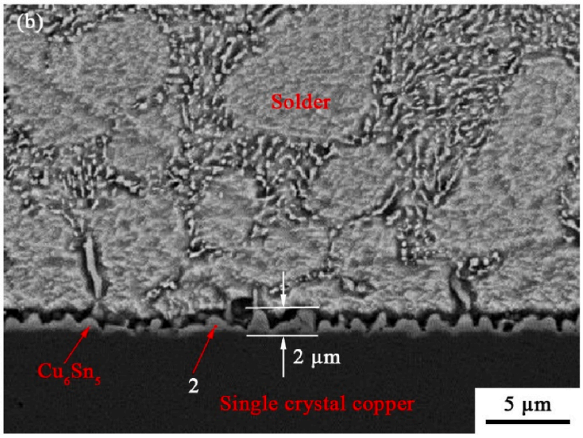

Fig. 2. Interface morphology of Sn-1.5Ag-2.0Zn alloy solder refluxed with different copper substrates at 250 °C for 5 min: (a) polycrystalline red copper (b) single crystal (111) copper

Table 1
Fig. 2 EDX analysis results.

Point code	Atomic %				Phase indentification
	Sn	Ag	Zn	Cu	
1	49.32	1.31	1.13	48.24	Cu_6Sn_5
2	45.24	2.14	3.28	49.34	Cu_6Sn_5

3.2. Microstructure evolution of the interface between solder and different copper substrates

In order to study the evolutionary characteristics of the IMCs at the solder joints of Sn-1.5Ag-2.0Zn and polycrystalline copper with the change of aging treatment time, the solder joints of Sn-1.5Ag-2.0Zn and polycrystalline copper were placed in a constant temperature drying oven at 160 °C and aged for 20 h, 100 h, 300 h and 600 h. The samples were heat-treated at 160 °C for 20 h, 100 h, 300 h, and 600 h. The organization and morphology of the interface of the solder joints obtained are shown in Fig. 4(a)–(b), Fig. 4(c), and Fig. 4(d). It was found that with the increase of aging treatment time, the originally uneven IMC interface tended to flatten out and increase in thickness. After 20 h aging, the IMC at the interface starts to show a layered structure. After 100 h aging, the IMC at the interface has a clear delamination boundary, as shown at the dashed line in Fig. 4(b). Linear scanning analysis of the elemental distribution near the A-B interface in Fig. 4(b) was performed using EDS, and the results are shown in Fig. 4(e). Ag and Zn elements are enriched at the interface. Combined with the elemental distribution, it can be judged that the interface layer consists of a mixture of fine Ag–Sn and Cu–Zn IMC. Fig. 4(f) shows the top view of the SEM interface after 100 h of aging, and it is found that the protruding granular IMCs are Ag_3Sn, and the flatter IMCs below the granular IMCs are mainly Cu_5Zn_8. This result is also consistent with the scanning photographs of the interface cross section. The morphology of the IMC evolved on a bilayer structure until the aging time was increased to 600 h. An EDS linear scan of the elemental distribution near the C-D interface in Fig. 4(d) is shown in Fig. 4(g). The

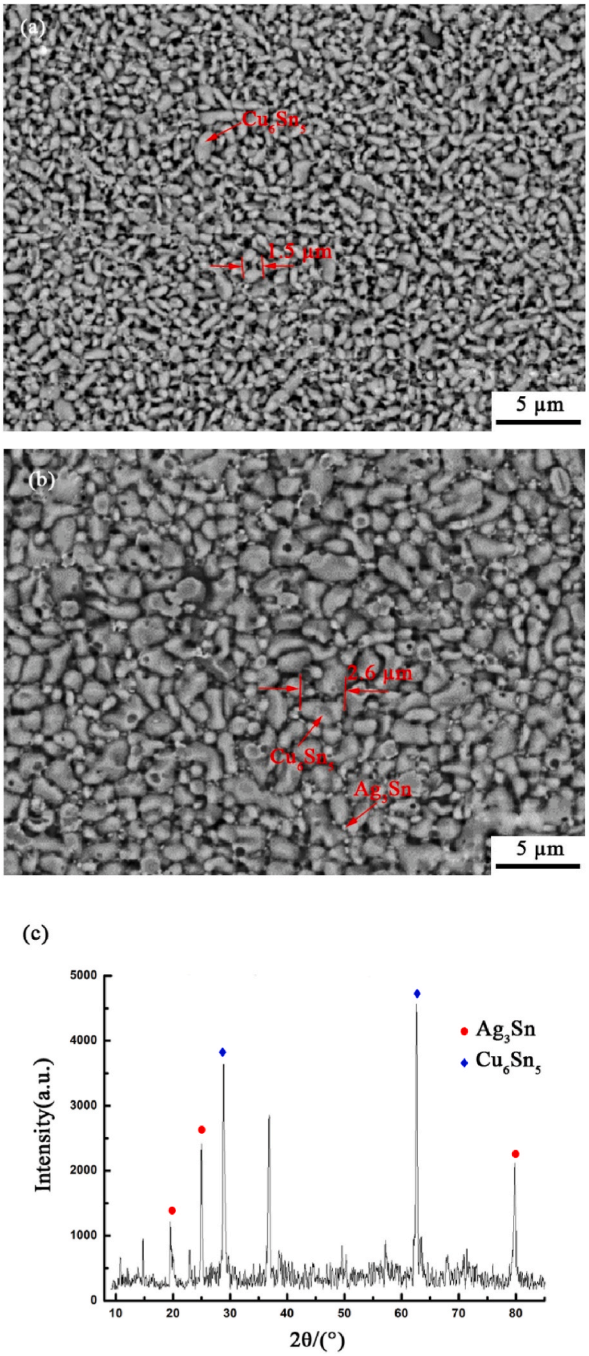

Fig. 3. Top view of Sn-1.5Ag-2.0Zn alloy solder refluxed at 250 °C with different copper substrates for 5 min: (a) polycrystalline red copper (b) single crystal (111) copper (c) XRD pattern of solder and single crystal copper interface

separation of Ag_3Sn and Cu_5Zn_8 and the generation of Cu–Sn IMCs can be seen more clearly. The EDX analysis of points 1, 2, 3 and 4 in Fig. 4 (Table 2) shows that Ag_3Sn covered the top of Cu_5Zn_8 with a thickness of about 1.5 μm after 100 h of aging. The thickness and flatness of Cu_5Zn_8 were relatively stable after 300 h of aging. It was clear that the presence of Cu_5Zn_8 limited the growth of Cu_6Sn_5. Cu_5Zn_8 decomposed to produce Cu_6Sn_5 after aging for 600 h. The thickness of the generated IMC (Ag_3Sn, Cu_6Sn_5) after aging treatment for 600 h was about 2.8 μm.

At the interface of the specimen after 600 h aging, some areas where the solder severely eroded the substrate were found. As in Fig. 5(a), Sn eroded deep into the polycrystalline copper substrate. Since Sn tends to corrode away during metallographic etching, pits can be seen in Fig. 5(b), along with fine IMC phases distributed in the Sn. EDS elemental analysis (Table 2) is performed on the bottom

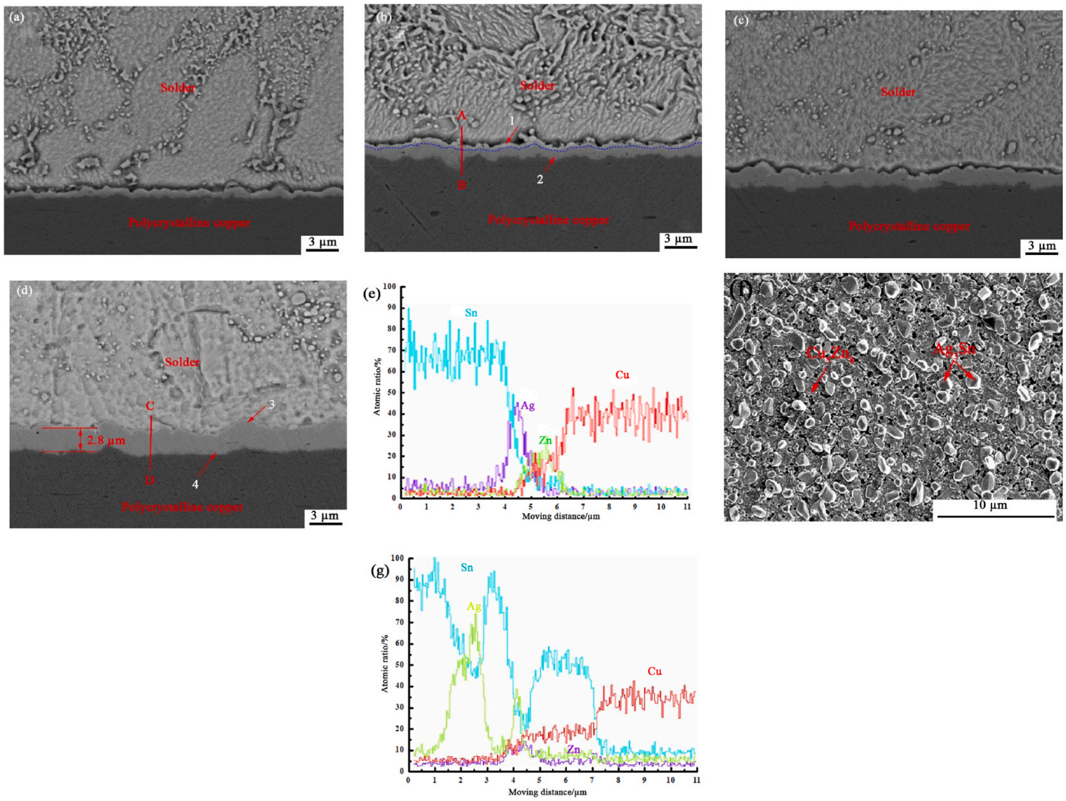

Fig. 4. Microstructure of Sn-1.5Ag-2.0Zn alloy solder/polycrystalline copper solder joint at 160 °C with different aging treatment time: (a) 20 h (b) 100 h (c) 300 h (d) 600 h (e) Linear scanning analysis of A-B (f) Top view of morphology (g) Linear scanning analysis of C-D.

Table 2
EDX analysis results.

Point code	Atomic %				Phase indentification
	Sn	Ag	Zn	Cu	
1	19.98	20.88	27.72	31.42	$Ag_3Sn + Cu_5Zn_8$
2	1.12	3.16	62.05	33.67	Cu_5Zn_8
3	42.38	22.57	2.98	32.07	Cu_6Sn_5+Ag_3Sn
4	46.34	2.34	3.04	48.28	Cu_6Sn_5
5	38.34	1.28	7.56	52.82	Cu_6Sn_5

of the holes (on the point 5), and with reference to the atomic ratio of Sn to Cu, it can be inferred that it mainly forms Cu–Sn IMCs, and it is mainly Cu_6Sn_5.

Fig. 6 shows the results of TEM analysis of the interface between the Sn-1.5Ag-2.0Zn alloy solder and the polycrystalline copper substrate at 160 °C for 300 h. The selected electron diffraction pattern in the A region corresponds to Cu_6Sn_5 with a crystalline band axis of [0 1 0]. The selected electron diffraction pattern in the C region corresponds to Cu_6Sn_5 with a crystalline band axis of [2–12], and the selected electron diffraction pattern in the B region corresponds to Cu_5Zn_8 with a crystalline band axis of [0−1 0]. It can be found that the rod-shaped particles A-phase Cu_6Sn_5 and B-phase Cu_5Zn_8 are grown in polycrystalline copper substrate nucleation. The C phase Cu_6Sn_5 can be nucleated and grown on B phase Cu_5Zn_8. It can be concluded that the interface layer mainly consists of a mixture of Cu_6Sn_5 and Cu_5Zn_8 phases, and with the extension of aging Cu_5Zn_8 has a tendency to decompose and transform into Cu_6Sn_5.

In order to further investigate the evolution characteristics of the IMCs at the solder joints of Sn-1.5Ag-2.0Zn and single-crystal copper with the changes in aging treatment time, the solder joints of Sn-1.5Ag-2.0Zn and single-crystal copper (111) were placed in a constant temperature drying oven at 160 °C and aged for 20 h, 100 h, 300 h, and 600 h. The organization and morphology of the solder joint interface obtained after aging treatment at 160 °C for 20 h, 100 h, 300 h and 600 h are shown in Fig. 7(a)–(b), Fig. 7(c) and (d), respectively. It was found Cu_6Sn_5 was bulky at the solder interior, and the Cu_6Sn_5 IMC was formed rapidly at the solder interface, whose thickness increased with the increase of aging treatment time. However, the growth of the IMC was slow and the thickness of the IMC at the interface was about 3.3 μm after 300 h of aging treatment. In Fig. 7(a), significant cracks began to appear above the IMC layer after 20 h of aging treatment, mainly due to the IMC was hard and brittle properties, which is prone to cracking under stress. In

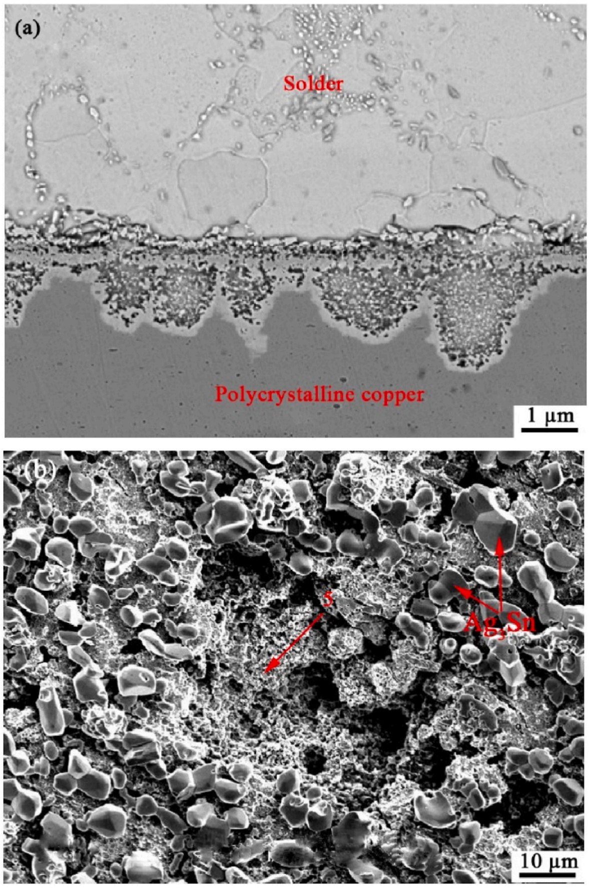

Fig. 5. Solder erosion of the substrate: (a) interface morphology (b) secondary electron top view morphology.

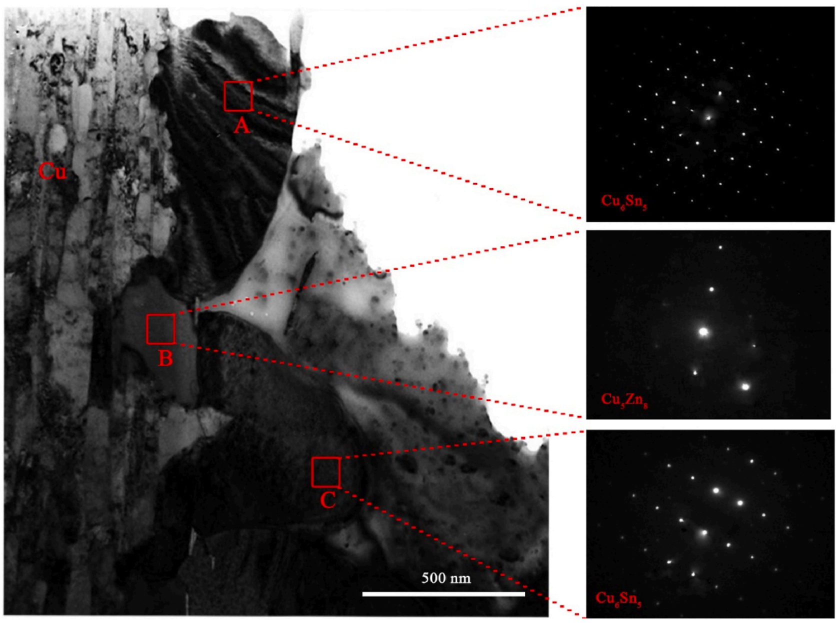

Fig. 6. TEM analysis of the interface between Sn-1.5Ag-2.0Zn alloy solder and polycrystalline copper substrate with aging at 160 °C for 300 h.

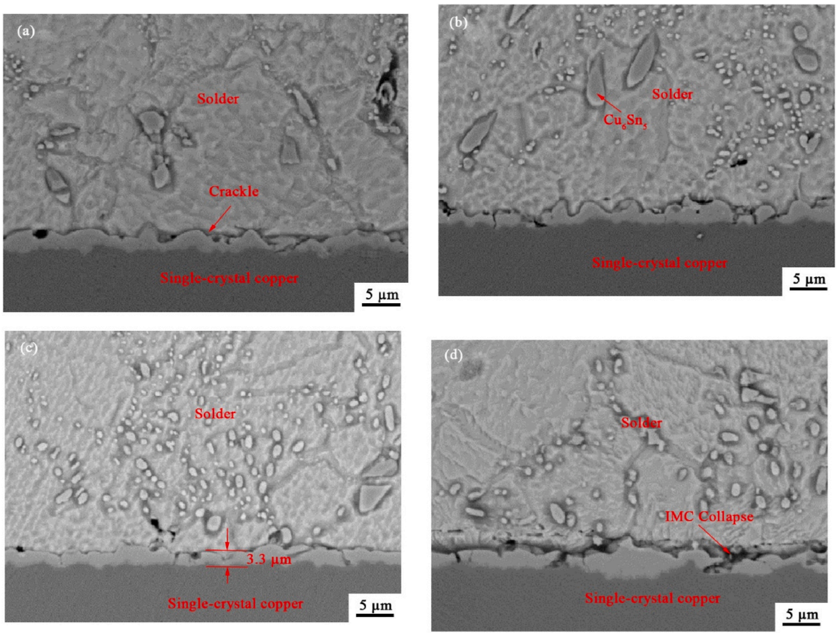

Fig. 7. Microstructure of Sn-1.5Ag-2.0Zn alloy solder/single crystal copper (111) solder joint at 160 °C at different aging treatment times: (a) 20 h (b) 100 h (c) 300 h (d) 600 h.

Fig. 7(d), the cracks spread sharply after 600 h of aging treatment, and the thick IMC layer at the soldering interface appeared collapse phenomenon.

To investigate the reliability of the solder joints of Sn-1.5Ag-2.0Zn soldered to single crystal Cu (111) substrates, the interface IMC thicknesses were counted for different aging times (20 h, 100 h, 300 h and 600 h) after soldering. For the thickness measurements, typical interface photographs were selected and the thickness values were calculated by averaging the values of nine randomly selected locations after removing the maximum and minimum values. Table 3 shows the statistical table of IMC thickness obtained after different aging treatment times at 160 °C. It can be presumed that the IMC thickness of the soldering interface after a long aging treatment was stable at about 3.5 μm.

The commercial solder Sn-3.0Ag-0.5Cu (SAC305) was chosen for the comparison experiments. The samples soldered with SAC305 solder and single crystal copper (111) were aged at 160 °C for 20 h, 100 h, 300 h, and 600 h. The interfacial morphology of the solder joints was observed as shown in Fig. 8(a)–(b), Fig. 8(c), and Fig. 8(d). It was found that the thickness of the Cu–Sn IMC layer at the interface of Sn-3.0Ag-0.5Cu/single crystal copper (111) increased rapidly with increasing aging time. Cracks were found inside the IMC layer at the interface after 600 h aging treatment. The interface IMC thickness reached 7.28 μm after 300 h aging treatment, as shown in Table 4, which is about more than two times the thickness of the IMC at the Sn-1.5Ag-2.0Zn/single-crystal Cu (111) interface. This thick IMC layer will adversely affect the mechanical properties of the solder joint.

Fig. 9 shows the top-view morphology of the interface solder joint after aging treatment at 160 °C for 20 h. It can be found that the IMC grown on single-crystal copper has a clustered prismatic distribution, while the IMC grown on polycrystalline copper has a haphazard ellipsoidal distribution. Fig. 9(a) shows the solder joint between the alloy solder and the single crystal copper (111). It was found that the Cu_6Sn_5 grains grew significantly after aging treatment. The grain boundaries between the grains were clearly defined. The uneven IMC layer before heat treatment tends to be flattened by thermal diffusion. The height of IMC grains are basically the same, and the height difference is significantly reduced. the IMC density is good, and there are basically no intergranular holes. By observation, white particles can be found on Cu_6Sn_5. This should be Ag_3Sn nanoparticles that have grown up after aging. During the ultrasonic cleaning process, some Ag_3Sn particles were dislodged and formed holes on Cu_6Sn_5.

Comparing the IMC layer at the interface between the alloy solder and polycrystalline copper in Fig. 9(b), it was found that holes due to the dislodged Ag_3Sn particles are also present on Cu_6Sn_5 at the interface between the alloy solder and polycrystalline copper. In

Table 3
Thickness of IMC at the interface of Sn-1.5Ag-2.0Zn alloy solder/single crystal copper (111) under different aging treatment time at 160 °C.

Aging treatment time/h	IMC thickness average/μm
20	2.87
100	2.98
300	3.30
600	3.47

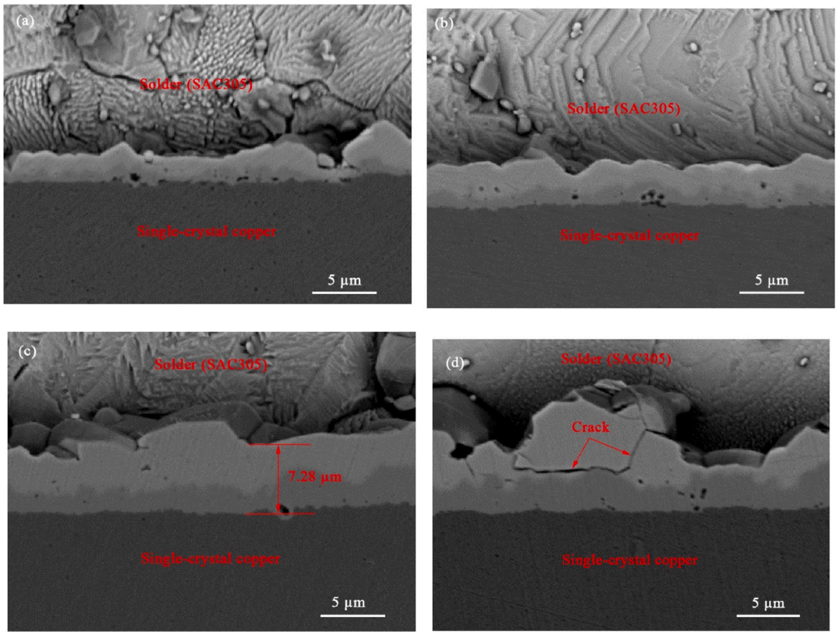

Fig. 8. Microstructure of Sn-3.0Ag-0.5Cu alloy solder/single crystal copper (111) solder joint at 160 °C at different aging treatment times: (a) 20 h (b) 100 h (c) 300 h (d) 600 h.

Table 4
Thickness of IMC at the interface of Sn-3.0Ag-0.5Cu alloy solder/single crystal copper (111) under different aging treatment time at 160 °C.

Aging treatment time/h	IMC thickness average/μm
20	2.62
100	4.23
300	7.28
600	11.12

addition to this, there were also obvious intergranular holes. Comparing with Fig. 8(a), it is obvious that the IMC formed at the interface between the alloy solder and the single-crystal copper has better densification, and there is basically no intergranular holes. It can be predicted that the solder quality at the interface between alloy solder and single-crystal copper is better.

Fig. 10 shows the thickness of the IMC formed between the interface of the alloy solder and the different copper substrates as a function of the aging treatment time. The horizontal coordinate is the square root of the aging treatment time. The horizontal coordinate is the square root of the aging treatment time, and it was found that the thickness of the IMC remains essentially linear with the square root of the aging treatment time, which is in accordance with the diffusion law. The growth rate of IMCs within the aging treatment time of 0–20 h on single-crystal copper (111) was significantly faster than that on polycrystalline copper, which was about twice as fast as that on polycrystalline copper. The growth rate of IMCs on polycrystalline copper was accelerated after 100 h of aging treatment time, which should be caused by the dissolution of Cu_5Zn_8 barrier layer. The thickness of the IMC on single-crystal copper (111) was slightly thicker than that on polycrystalline copper by 0.7 μm after 600 h of aging treatment time. The growth process of IMC at the interface of Sn-3.0Ag-0.5Cu/single crystal copper (111) was found to be in accordance with the parabolic growth law, i.e., the growth of IMC is controlled by diffusion. The growth rate of IMC is very large after 20 h aging, and the solder erodes the substrate to form a thick layer of Cu–Sn IMC, which has a negative impact on the reliability of the solder joint.

4. Conclusion

(1) A layer of Cu_6Sn_5 IMCs with an uneven, scallop-like shape grew rapidly at the interface between the Sn-1.5Ag–2Zn alloy solder and the copper substrate. The grain size of Cu_6Sn_5 formed on the surface of single-crystal copper was about 2.6 μm in diameter, while the grain size of Cu_6Sn_5 formed on the surface of polycrystalline copper was about 1.5 μm in diameter. it is obvious that the grain size of Cu_6Sn_5 formed on the surface of single-crystal copper is larger than that of polycrystalline copper. This is due to the absence of grain boundaries in single-crystal copper, and the existence of grain boundaries has a certain effect on grain nucleation and growth.

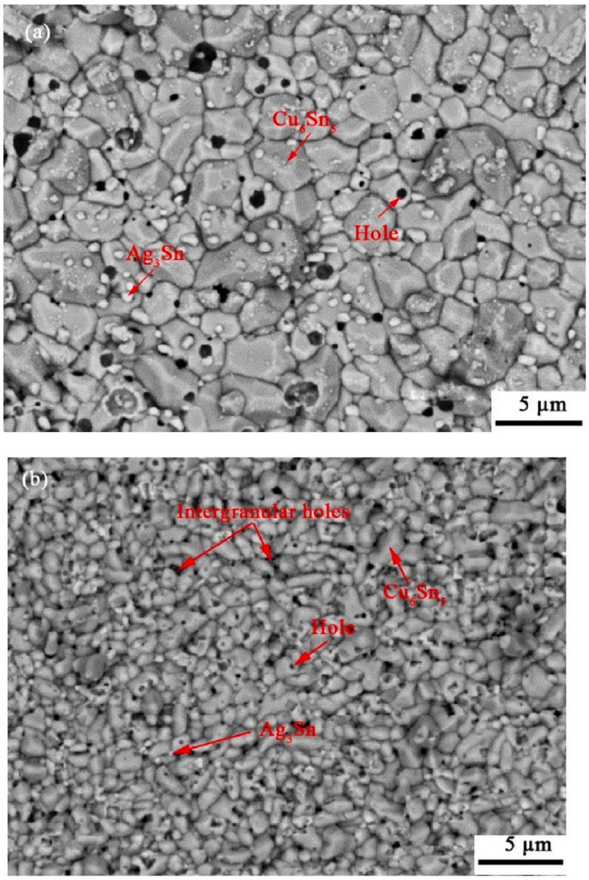

Fig. 9. Top view morphology and structure of IMC at the interface solder joint after aging treatment at 160 °C for 20 h: (a) Sn-1.5Ag-2.0Zn alloy solder/single-crystal copper (111) (b) Sn-1.5Ag-2.0Zn alloy solder/polycrystalline copper.

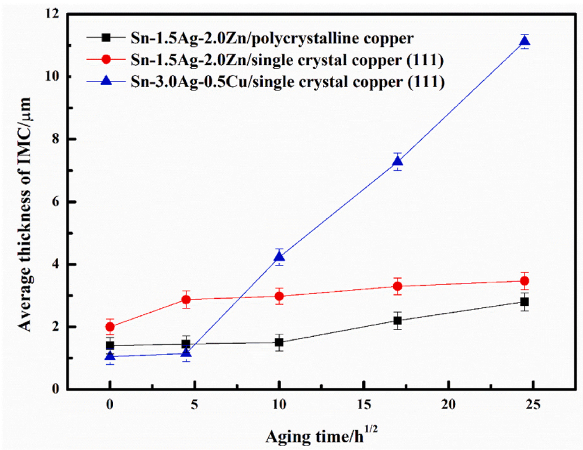

Fig. 10. Relationship between the thickness of the IMC and aging treatment time.

(2) Cu_5Zn_8 IMCs were formed in the solder joints between Sn-1.5Ag–2Zn solder and polycrystalline copper substrates during heat treatment at 160 °C. These compounds acted as a barrier layer between the solder and the copper substrate to inhibit the formation of Cu_6Sn_5. After 24 h of heat treatment, the IMCs showed a layered structure. After 100 h of heat treatment, Ag_3Sn covered the top of Cu_5Zn_8 with a thickness of about 1.5 μm. After 600 h of heat treatment, the Cu_5Zn_8 IMCs decomposed and the Cu_6Sn_5 grew rapidly with a thickness of about 2.8 μm.

(3) The thickness of the IMCs were 2.87 μm after a short heat treatment of Sn-1.5Ag–2Zn alloy solder and single crystal (111) copper substrate at 160 °C for 20 h. The growth rate of the IMCs are about two times that of the polycrystalline copper substrate. The thickness of the IMCs grew slowly with the increase of heat treatment time. After 600 h of heat treatment, the thickness of the IMCs were about 3.5 μm, and the thick layer of IMC collapsed due to crack expansion.

Funding statement

This study was funded by the Guangzhou Zengcheng District Science and Technology Planning Project (NO:2021ZCMS11).

Data availability statement

Data will be made available on request.

CRediT authorship contribution statement

Jin Xiao: Funding acquisition, Formal analysis, Conceptualization. **Wei Cheng:** Investigation. **Qu Fu-kang:** Software.

Declaration of competing interest

The authors declare that they have no known competing financial interests or personal relationships that could have appeared to influence the work reported in this paper.

References

[1] Z. Yao, D. Ling, Y. Liu, J. Sun, L. Yin, G. Wang, L. Zhang, Effect of Cu addition on the microstructure and mechanical properties of Sn-58Bi-0.5Ag solder alloys, J. Electron. Mater. 51 (7) (2022) 3552–3559, https://doi.org/10.1007/s11664-022-09601-y.
[2] J. Xiao, X. Tong, J. Liang, Q. Chen, Q. Tang, Microstructure and morphology of the soldering interface of Sn–2.0Ag–1.5Zn low Ag content lead-free solder ball and different substrates, Heliyon 9 (2) (2023) e12952, https://doi.org/10.1016/j.heliyon.2023.e12952.
[3] Y. Fan, Y. Wu, T.F. Dale, S.A.P. Lakshminarayana, C.V. Greene, N.U. Badwe, R.F. Aspandiar, J.E. Blendell, G. Subbarayan, C.A. Handwerker, Influence of pad surface finish on the microstructure evolution and intermetallic compound growth in homogeneous Sn-Bi and Sn-Bi-Ag solder interconnects, J. Electron. Mater. 50 (12) (2021) 6615–6628, https://doi.org/10.1007/s11664-021-09256-1.
[4] D. Qi, W.c. Yang, H. Zhao, L. Zhang, S.w. Jiang, Q.q. Song, Y.k. Fu, Y.z. Zhan, Effects of Cu and in on the microstructure evolution and mechanical properties of Sn-20Bi/Cu solder joints, J. Mater. Sci. Mater. Electron. 34 (6) (2023) 503, https://doi.org/10.1007/s10854-022-09593-9.
[5] K.-K. Xu, L. Zhang, L.-L. Gao, N. Jiang, L. Zhang, S.-J. Zhong, Review of microstructure and properties of low temperature lead-free solder in electronic packaging, Sci. Technol. Adv. Mater. 21 (1) (2020) 689–711, https://doi.org/10.1080/14686996.2020.1824255.
[6] H. Kang, A. Sharma, J.-H. Lee, J.P. Jung, Transient liquid phase bonding of silicon and direct bond copper via electroplating of tin-copper interlayers for power device applications, Mater. Res. Express 8 (1) (2021) 016301, https://doi.org/10.1088/2053-1591/abd5d9.
[7] F. Wang, H. Chen, Y. Huang, L. Liu, Z. Zhang, Recent progress on the development of Sn–Bi based low-temperature Pb-free solders, J. Mater. Sci. Mater. Electron. 30 (4) (2019) 3222–3243, https://doi.org/10.1007/s10854-019-00701-w.
[8] S. Li, X. Wang, Z. Liu, Y. Jiu, S. Zhang, J. Geng, X. Chen, S. Wu, P. He, W. Long, Corrosion behavior of Sn-based lead-free solder alloys: a review, J. Mater. Sci. Mater. Electron. 31 (12) (2020) 9076–9090, https://doi.org/10.1007/s10854-020-03540-2.
[9] N. Jiang, L. Zhang, L.-L. Gao, X.-G. Song, P. He, Recent advances on SnBi low-temperature solder for electronic interconnections, J. Mater. Sci. Mater. Electron. 32 (18) (2021) 22731–22759, https://doi.org/10.1007/s10854-021-06820-7.
[10] W. Qin, J. Li, Q. Zhang, S. Jiang, J. Feng, W. Yang, Y. Zhan, Effect of addition of Al and Cu on the properties of Sn–20Bi solder alloy, J. Mater. Sci. Mater. Electron. 33 (1) (2022) 177–189, https://doi.org/10.1007/s10854-021-07283-6.
[11] S. Tian, S. Li, J. Zhou, F. Xue, Thermodynamic characteristics, microstructure and mechanical properties of Sn-0.7Cu-xIn lead-free solder alloy, J. Alloys Compd. 742 (2018) 835–843, https://doi.org/10.1016/j.jallcom.2018.01.386.
[12] G. Chen, X.H. Wang, J. Yang, W.L. Xu, Q. Lin, Effect of micromorphology on corrosion and mechanical properties of SAC305 lead-free solders, Microelectron. Reliab. 108 (2020) 113634, https://doi.org/10.1016/j.microrel.2020.113634.
[13] S. Liu, T. Song, W. Xiong, L. Liu, Z. Liu, S. Huang, Effects of Ag on the microstructure and shear strength of rapidly solidified Sn–58Bi solder, J. Mater. Sci. Mater. Electron. 30 (7) (2019) 6701–6707, https://doi.org/10.1007/s10854-019-00981-2.
[14] Z. Wang, Q.K. Zhang, Y.X. Chen, Z.L. Song, Influences of Ag and in alloying on Sn-Bi eutectic solder and SnBi/Cu solder joints, J. Mater. Sci. Mater. Electron. 30 (20) (2019) 18524–18538, https://doi.org/10.1007/s10854-019-02206-y.
[15] A.A. El-Daly, A.A. Ibrahiem, M.A. Abdo, N.A.M. Eid, Viscoplastic characterization and mechanical strength of novel Sn–1.7Ag–0.7Cu lead-free solder alloys with microalloying of Te and Co, J. Mater. Sci. Mater. Electron. 30 (14) (2019) 12937–12949, https://doi.org/10.1007/s10854-019-01656-8.
[16] A.T. Tan, A.W. Tan, F. Yusof, Evolution of microstructure and mechanical properties of Cu/SAC305/Cu solder joints under the influence of low ultrasonic power, J. Alloys Compd. 705 (2017) 188–197, https://doi.org/10.1016/j.jallcom.2017.02.165.
[17] Y. Yao, X. Yu, Thermal cycling aging effects on the tensile property and constitute behavior of Sn–3.0Ag–0.5Cu solder alloy, J. Mater. Sci. Mater. Electron. 30 (1) (2019) 867–875, https://doi.org/10.1007/s10854-018-0358-5.
[18] P. Jattakul, T. Madsa, P. Sunasuan, N. Mookam, Influence of cooling conditions on microstructure and mechanical property of Sn-0.3Ag-0.7Cu lead-free solder, Journal of Metals, Materials and Minerals 31 (2) (2021) 129–136, https://doi.org/10.55713/jmmm.v31i2.1085.
[19] M. Yadav, T. Alghoul, S. Thekkut, R. Das, C. Greene, P. Borgesen, A.R.N. Sakib, L. Wentlent, S. Joshi, Strength and isothermal fatigue resistance of SnBi/SnAgCu joints reflowed at low temperatures, J. Electron. Packag. 144 (3) (2021) 031001, https://doi.org/10.1115/1.4051620.
[20] Y. Su, R. Zhu, T. Zheng, Y. Shen, Y. Xu, L. Chen, Y. Zhang, C. Song, H. Zheng, Q. Zhai, Intermetallic compounds formed in Sn droplet on Cu substrate under the impact of electric currents, J. Mater. Sci. 56 (2021) 11953–11969, https://doi.org/10.1007/s10853-021-06048-0.
[21] P. Zhang, S. Xue, L. Liu, J. Wang, H. Tatsumi, H. Nishikawa, Influence of isothermal aging on microstructure and shear property of novel epoxy composite SAC305 solder joints, Polymers 15 (20) (2023) 4168, https://doi.org/10.3390/polym15204168.
[22] L. Yin, Z. Zhang, C. Zuo, N. Fang, Z. Yao, Z. Su, Microstructures and properties of Sn–0.3Ag–0.7Cu solder doped with graphene nanosheets, J. Mater. Sci. Mater. Electron. 31 (3) (2020) 1861–1867, https://doi.org/10.1007/s10854-019-02705-y.
[23] P. Tunthawiroon, K. Kanlayasiri, Effects of Ag contents in Sn–xAg lead-free solders on microstructure, corrosion behavior and interfacial reaction with Cu substrate, Trans. Nonferrous Metals Soc. China 29 (8) (2019) 1696–1704, https://doi.org/10.1016/S1003-6326(19)65076-4.

[24] B. Lin, G. Lu, H. Wang, J. Yuan, F. Wei, Y. Sui, J. Qi, Q. Meng, Y. Ren, Novel Sn-0.7 Cu composite solder reinforced with ultrafine nanoscale nickel particles/porous carbon, Mater. Char. 194 (2022) 112414, https://doi.org/10.1016/j.matchar.2022.112414.
[25] M. Yadav, T. Alghoul, S. Thekkut, R. Das, C. Greene, P. Borgesen, A.R.N. Sakib, L. Wentlent, S. Joshi, Strength and isothermal fatigue resistance of SnBi/SnAgCu joints reflowed at low temperatures, J. Electron. Packag. 144 (3) (2022) 031001, https://doi.org/10.1115/1.4051620.
[26] Y. Su, R. Zhu, T. Zheng, Y. Shen, Y. Xu, L. Chen, Y. Zhang, C. Song, H. Zheng, Q. Zhai, Intermetallic compounds formed in Sn droplet on Cu substrate under the impact of electric currents, J. Mater. Sci. 56 (2021) 11953–11969, https://doi.org/10.1007/s10853-021-06048-0.
[27] H. Chen, T.-T. Chou, C. Fleshman, J.-G. Duh, Investigating the effect of Ag content on mechanical properties of Sn-Ag-Cu micro-BGA joints, J. Electron. Mater. 48 (10) (2019) 6866–6871, https://doi.org/10.1007/s11664-019-07428-8.
[28] X. Ren, Y. Wang, L. Zou, X. Liu, N. Zhao, Effects of size and cooling rate on solidification behavior of freestanding Sn-3.0Ag-0.5Cu solder balls, Mater. Char. 182 (2021) 111530, https://doi.org/10.1016/j.matchar.2021.111530.
[29] A.E. Hammad, M. Ragab, Achieving microstructure refinement and superior mechanical performance of Sn-2.0Ag-0.5Cu-2.0Zn (SACZ) solder alloy with rotary magnetic field, Microelectron. Reliab. 113 (2020) 113932, https://doi.org/10.1016/j.microrel.2020.113932.
[30] T. Zhu, Q. Zhang, H. Bai, L. Zhao, J. Yan, Improving tensile strength of SnAgCu/Cu solder joint through multi-elements alloying, Mater. Today Commun. 29 (2021) 102768, https://doi.org/10.1016/j.mtcomm.2021.102768.
[31] Y. Li, W. Lin, X. Li, H. Ouyang, Effects of Zn contents on microstructure, thermodynamic characteristic and mechanical properties of Sn–Bi-based lead-free solder, J. Mater. Sci. Mater. Electron. 33 (4) (2022) 1741–1751, https://doi.org/10.1007/s10854-021-07153-1.
[32] X. Zeng, Y. Liu, J. Zhang, Y. Liu, X. Hu, X. Jiang, Effect of rare earth Ce on the thermal behavior, microstructure and mechanical properties of Zn–30Sn–2Cu high temperature lead-free solder alloy, J. Mater. Sci. Mater. Electron. 31 (19) (2020) 16437–16447, https://doi.org/10.1007/s10854-020-04196-8.
[33] L.S. Ramos, R.V. Reyes, L.F. Gomes, A. Garcia, J.E. Spinelli, B.L. Silva, The role of eutectic colonies in the tensile properties of a Sn–Zn eutectic solder alloy, Mater. Sci. Eng., A 776 (2020) 138959, https://doi.org/10.1016/j.msea.2020.138959.
[34] E.A. Eid, A.B. El-Basaty, A.M. Deghady, S. Kaytbay, A. Nassar, Influence of nano-metric Al2O3 particles addition on thermal behavior, microstructural and tensile characteristics of hypoeutectic Sn-5.0Zn-0.3Cu Pb-free solder alloy, J. Mater. Sci. Mater. Electron. 30 (4) (2019) 4326–4335, https://doi.org/10.1007/s10854-019-00726-1.
[35] Y. Wei, Y. Liu, L. Zhang, X. Zhao, Effects of endogenous Al and Zn phases on mechanical properties of Sn58Bi eutectic alloy, Mater. Char. 175 (2021) 111089, https://doi.org/10.1016/j.matchar.2021.111089.
[36] S. Zhou, O. Mokhtari, M.G. Rafique, V.C. Shunmugasamy, B. Mansoor, H. Nishikawa, Improvement in the mechanical properties of eutectic Sn58Bi alloy by 0.5 and 1 wt% Zn addition before and after thermal aging, J. Alloys Compd. 765 (2018) 1243–1252, https://doi.org/10.1016/j.jallcom.2018.06.121.
[37] Y. Qiao, X. Liu, N. Zhao, L.C.M. Wu, C. Liu, H. Ma, Morphology and orientation evolution of Cu6Sn5 grains on (001)Cu and (011)Cu single crystal substrates under temperature gradient, J. Mater. Sci. Technol. 95 (2021) 29–39, https://doi.org/10.1016/j.jmst.2021.03.065.
[38] Y.Y. Qiao, N. Zhao, C.Y. Liu, C.M.L. Wu, Y.P. Wang, H.T. Ma, Dramatic morphological reservation of prism-type Cu6Sn5 formed on single crystal Cu substrates under temperature gradient, Mater. Today Commun. 23 (2020) 100928, https://doi.org/10.1016/j.mtcomm.2020.100928.
[39] H.R. Ma, C. Dong, J. Chen, Y.P. Wang, X.G. Li, H.T. Ma, Mechanism and control of preferred Cu6Sn5 growth on single crystal (001)Cu, J. Mater. Sci. Mater. Electron. 31 (8) (2020) 5966–5974, https://doi.org/10.1007/s10854-020-03150-y.
[40] C. Dong, M. Shang, F. Chen, Y. Wang, X. Li, H. Ma, H. Ma, Investigation on growth of the orientation-preferred Cu6Sn5 on (001)Cu during the temperature-increased multiple reflow process, J. Alloys Compd. 885 (2021) 161205, https://doi.org/10.1016/j.jallcom.2021.161205.